Supporting Information

Bao et al. 10.1073/pnas.1205978109

SI Materials and Methods

Current Annealing. We fabricate suspended bilayer graphene (BLG) devices with single or double gates (1, 2). Single-gated devices are fabricated without lithography, allowing high throughput and yielding exceedingly high-mobility samples. Double-gated geometry allows independent adjustment of induced charge density n and perpendicular electric field $E_\perp$ (3).

After fabrication we transfer our suspended BLG devices into a high-vacuum cryostat, and current annealing is performed at 1.5 K. A typical procedure is shown in Fig. S1. We first ramp up the source-drain bias V_{sd} at a rate of approximately 10 mV/s, and monitor the current I across the device, while keeping the gate electrode(s) grounded. The I-V curve, which is linear at low bias, becomes sublinear at larger bias (Fig. S1*A*). At this point V_{sd} is ramped down to zero, and we examine the field-effect mobility μ and minimum conductivity σ_{min} (Fig. S1*A*, *Inset*). Generally μ increases significantly and σ_{min} decreases. Several cycles of current annealing are performed until current saturation is observed (Fig. S1 *B* and *C*) and there is no further change in μ or σ_{min}; at this point the optimal annealing result is attained. If V_{sd} is increased further, the suspended membrane will begin to degrade due to electromigration, and μ will decrease again.

We also note that the annealing process is typically different for single-layer, bilayer, and trilayer (4) suspended graphene devices. For instance, current saturation is not reliably observed in the single-layer graphene during the annealing process.

Device Mobility Metrics. BLG devices are characterized by their field-effect mobility values, $\mu_{FE} = \frac{1}{e}\frac{d\sigma}{dn}$, where e is the electron charge, σ is the conductivity, and n is the charge density. μ_{FE} is typically measured by taking the slope of a raw $\sigma(n)$ curve between $n = 0$ and n of approximately 2×10^{10} cm^{-2}, without subtracting any series resistance (apart from the known line resistance of the refrigerator). We find that μ_{FE} values are inversely proportional to the full width at half maximum (FWHM) Γ of the $\rho(n)$ curves, where $\rho = 1/\sigma$ is the resistivity, as shown in Fig. S2.

Another commonly used metric of device quality is the so-called "quantum mobility" μ_q defined in terms of the inverse magnetic field value at which Shubnikov–de Haas oscillations are first observed. Because most of our devices were not measured in magnetic field B, or not with a sufficiently high B resolution to allow μ_q to be accurately determined, this metric is not used to characterize our samples. Nevertheless, for a few devices in which μ_q has been measured accurately, we find that it is larger than μ_{FE} by a factor that ranges from 50% to 200%. Thus, it appears that our μ_{FE} values are lower-bound characterizations of device quality.

Quantum Hall Effect (QHE) in Suspended BLG With and Without Insulating State. The QHE is observed in all suspended BLG devices with sufficiently high mobility. The Landau fan diagrams of an insulating and a conducting sample are compared in Fig. 1 *D* and *E* (*Insets*) in the main text, and their line traces $G(V_{bg})$ at different magnetic field B are shown in Fig. S3 *A*–*D*. Both devices exhibit the anticipated integer QHE conductance plateaus at the integer multiples ± 16, ± 12, ± 8, and ± 4 of e^2/h at relatively low magnetic fields starting from around 0.5 Tesla. The low fields are indicative of the high quality of our suspended devices. At higher magnetic fields, quantum Hall plateaus with integer values 0, ± 1, ± 2, and ± 3 e^2/h (Fig. S3 *B* and *D*) are observed, indicating breaking of the eightfold degeneracy of the lowest Landau level.

Line traces of $G_{min}(B)$ taken at the CNP in Fig. 1 *D* and *E* (*Insets*) show that both types of suspended BLG exhibit insulating states at high magnetic field up to $10T$; for the suspended BLG that is conductive at $B = 0$, we observe a precipitous transition to an insulating state as B increases to approximately $1T$.

Temperature Dependence of $\sigma(V_{bg})$ for Suspended and Substrate-Supported BLG. Fig. S4 displays $\sigma(V_{bg})$ at different temperatures T for suspended insulating BLG, suspended non-insulating BLG, and substrate-supported BLG devices, respectively. We observe minimal T-dependence for the substrate-supported devices. For both suspended devices, σ at large doping is only weakly temperature-dependent, whereas σ at half-filling decreases sharply with temperature. In particular, $\sigma_{min}(T)$ of insulating BLG devices has the strongest T-dependence, falling by several orders of magnitudes to approximately 0.05 e^2/h.

Theoretical Discussion of Minimum Conductivity in Bilayer Graphene. The charge carriers in monolayer graphene are massless Dirac fermions. Although the possibility of density-wave order, which would open a gap in graphene's charged excitation spectrum, has been discussed theoretically (ref. 5 and references therein, 6), it does not appear to be realized experimentally (7). In BLG, on the other hand, there is increasing evidence for ordered electronic states. Quasiparticle properties provide a valuable, if indirect, probe of the symmetries that are broken in the ordered state. In particular, the minimum conductivity at the carrier neutrality is expected to behave quite differently in different candidate states.

When the trigonal warping process proportional to hopping parameter γ_3 is neglected, BLG is described by a chiral Hamiltonian that has a quadratic band touching (Dirac) point at momentum $p = 0$ measured from either K or K' Brillouin-zone corners. The spectrum is gapless, quadratic in p, and rotationally invariant. The band eigenstates have a phase difference between sublattices that changes by 4π when the quasiparticle momentum circles the Dirac point, a property we refer to as $J = 2$ vorticity. The minimum conductivity at charge neutrality is predicted to be approximately $(8/\pi)$ e^2/h for gapless BLG with quadratic dispersion (8–16), twice as large as in monolayer graphene.

When the band Hamiltonian is described using a two-band pseudospin language, band touching points are conveniently discussed in terms of the coefficients that appear in its Pauli matrix (σ_i) expansion, which can be interpreted for $i = 1$, 2, and 3 as momentum-dependent effective magnetic fields. Band touching points can be identified by setting all three components of the pseudospin field to zero. When trigonal warping is included in the band Hamiltonian the gap between conduction and valence bands vanishes at $p = 0$, and also at three additional $p = 0$ points. (See ref. 17 or ref. 18, supplement.) The central Dirac point at $p = 0$ has momentum-space pseudospin vorticity $J = -1$ whereas the finite $p = v_3\gamma_1/v_0^2$ points appear at angles $\Phi = 0$, $\pi/3$, and $2\pi/3$, and have $J = 1$. The in-plane $SO(2)$ rotational symmetry around each Dirac point is reduced to C_3 symmetry and the energy dispersion is linear near all the four Dirac cones. The trigonal warping effect dominates at energies below approximately 1 meV. Theories have predicted that when the disorder scale is weaker than approximately 1 meV, these band distortions will increase the minimum conductivity in BLG to approximately $(24/\pi)$ e^2/h (8, 12, 13), three times larger than in quadratic BLG and six times larger than in gapless monolayer graphene. It is not clear that disorder is actually sufficiently weak to reach this regime even in the highest-quality samples currently available

(i.e., for bilayers on h-BN substrates or current-annealed suspended bilayers). This strongly enhanced minimum conductivity should, however, apply for ideal samples with very weak disorder and no interactions.

The disorder-strength independent minimum conductivities in graphene-based two-dimensional electron systems most likely arise from scattering from smooth inhomogeneities, possibly randomly distributed charged impurities on the substrates, that produce electron-hole puddles (14). When electron-electron interactions are neglected, a nearly universal minimum conductivity is consistently predicted for BLG using self-consistent Born approximation, Kubo formula, Boltzmann's theory, and Landauer approaches to transport theory. The conductivity of BLG with nematic order has also been studied theoretically in recent work (16) motivated by predictions (19–21) that electron–electron interactions induce a gapless nematic state in BLG. In the nematic state the bilayer's in-plane rotational symmetry is spontaneously broken and the band structure topology has two $J = 1$ Dirac points. When trigonal warping is absent, the minimum conductivity of nematic BLG is $(8/\pi)\, e^2/h$, independent of the value of nematic order parameter and the quasiparticle lifetime (16). In the presence of trigonal warping, the minimum conductivity depends very sensitively on the orientation of the sample and on the strength and direction of nematic order. Generally $\sigma_{\min} \simeq (8/\pi)\, e^2/h$ holds, but near the phase boundary of Lifshitz transition, the conductivity can be even larger than $(24/\pi)\, e^2/h$ (16).

Broken symmetry states with gaps in the quasiparticle spectrum have also been predicted (22–28) in BLG. Some recent experiments (3, 4, 18, 29) appear to find evidence for gaps in suspended ultraclean samples. Because the low temperature transport properties of gapped and ungapped states differ qualitatively, these measurements can indirectly determine the type of order that is present in a system. The proposed gapped states are characterized by spontaneous charge transfer between layers, which minimizes exchange energies. When combined with the vortex-like momentum-space textures already present in the band structure, this insulating broken symmetry leads to large momentum-space Berry curvature and to quantized contribution to the Hall conductivity for each spin and valley (25). Three distinct spontaneous quantum Hall states with no overall layer polarization can be distinguished: a quantum anomalous Hall (QAH) state with broken time-reversal symmetry and quantized charge Hall conductivity; a quantum spin Hall (QSH) state with broken valley and spin symmetries; and a layer antiferromagnet (LAF) state with broken time-reversal and spin symmetries that have zero charge and spin Hall conductivities when the contributions from the two valleys are summed. Both the QAH and QSH states have topologically protected edge states that are expected to yield minimum (nonlocal) conductances of approximately 4 e^2/h. The edge states of the LAF state are only robust for perfect zigzag edges because valley index is not conserved. We therefore expect that $\sigma_{\min} \ll e^2/h$ in the LAF state. For this reason the LAF state is most consistent with small Dirac point conductances (18, 28). A separate gapped state that breaks layer-inversion symmetry is supported by a strong interlayer electric field. This state has opposite Hall conductivity in valley K and K' and is referred to as quantum valley Hall (QVH) state. The QVH edge state is not topologically protected, like LAF state, and its minimum conductance is thus expected to be much smaller than e^2/h. The BLG minimum conductances for various cases are summarized in Table S1.

Mean-Field Theory for the Influence of Carrier Density on Spontaneous Gap. When broken layer inversion symmetry physics occurs in suspended ultraclean BLG, the spontaneous gap $2m_s$ at zero carrier density can be obtained by solving the mean-field gap equation (25, 28),

$$m_s = \frac{V}{2A}\sum_k \frac{m_s}{\sqrt{\varepsilon_k^2 + m_s^2}}. \qquad \text{[S1]}$$

Here, $\varepsilon_k = -(v_0\hbar k)^2/\gamma_1$ is the non-interacting valence band energy, $v_0 = 10^6$ m/s is the Fermi velocity of a graphene sheet, $\gamma_1 = 400$ meV is the nearest-neighbor interlayer hopping energy, V is the effective interaction strength between electrons near the K or K' Brillouin-zone corners, and A is a sample area. When m_s is small compared to γ_1, the solution is given accurately by

$$m_s = 2\gamma_1 \exp(-2/\nu_0 V), \qquad \text{[S2]}$$

where $\nu_0 = \gamma_1/(4\pi\hbar^2 v_0^2)$ is the density of states in a single spin-valley. The spontaneous gap $2m_s = 2$ meV observed in experiment at zero magnetic field corresponds to a dimensionless interaction strength $\nu_0\, V = 0.2992$, close to the value expected to be appropriate for screened Coulomb interactions.

When the BLG carrier density is nonzero, it is possible to show that the temperature $T = 0$ mass is reduced to

$$m_s' = \sqrt{(m_s - \varepsilon_F)^2 - \varepsilon_F^2}, \qquad \text{[S3]}$$

because of Pauli blocking effects in the gap equation. Mean-field theory therefore predicts that the broken symmetry state disappears once Fermi energy becomes larger than $m_s/2 = 0.5$ meV, which corresponds to a carrier density larger than

$$n_c = 1.47 \times 10^{10}\ \text{cm}^{-2}. \qquad \text{[S4]}$$

Both the size of the gap at zero carrier density and the critical carrier density that destroys the gap are therefore roughly consistent with simple mean-field theory estimates. The smallness of the density fluctuation that destroys the gapped state is consistent with its appearance only in suspended samples.

Critical Temperature in Mean-Field Theory. The measured T_c at zero charge density and n_c at zero temperature are in good agreement with the mean-field theory results. The critical temperature at finite carrier density is determined by solving

$$\frac{2}{\nu_0 V} = \int_0^{\gamma_1} \frac{f_c(-\varepsilon-\mu) - f_c(\varepsilon-\mu)}{\varepsilon}\, d\varepsilon, \qquad \text{[S5]}$$

where $f_c(\varepsilon) = (1 + e^{\varepsilon/k_B T_c})^{-1}$ is the Fermi function at critical temperature T_c. The solution for the critical temperature T_c as a function of chemical potential and carrier density is plotted in Fig. S5.

1. Bao WZ, et al. (2010) Lithography-free fabrication of high quality substrate-supported and freestanding graphene devices. *Nano Res* 3:98–102.
2. Liu G, Velasco J, Bao WZ, Lau CN (2008) Fabrication of graphene *p-n-p* junctions with contactless top gates. *Appl Phys Lett* 92:203103.
3. Weitz RT, Allen MT, Feldman BE, Martin J, Yacoby A (2010) Broken-symmetry states in doubly gated suspended bilayer graphene. *Science* 330:812–816.
4. Bao W, et al. (2011) Stacking-dependent band gap and quantum transport in trilayer graphene. *Nat Phys* 7:948–952.
5. Drut JE, Lahde TA (2009) Is graphene in vacuum an insulator? *Phys Rev Lett* 102:026802.
6. Trushin M, Schliemann J (2011) Pseudospin in optical and transport properties of graphene. *Phys Rev Lett* 107:156801.
7. Elias DC, et al. (2011) Dirac cones reshaped by interaction effects in suspended graphene. *Nat Phys* 7:701–704.
8. Koshino M, Ando T (2006) Transport in bilayer graphene: Calculations within a self-consistent Born approximation. *Phys Rev B* 73:245403.
9. Snyman I, Beenakker CWJ (2007) Ballistic transmission through a graphene bilayer. *Phys Rev B* 75:045322.
10. Ziegler K (2007) Minimal conductivity of graphene: Nonuniversal values from the Kubo formula. *Phys Rev B* 75:233407.

11. Ryu S, Mudry C, Furusaki A, Ludwig AWW (2007) Landauer conductance and twisted boundary conditions for Dirac fermions in two space dimensions. *Phys Rev B* 75:205344.
12. Cserti J, Csordás A, Dávid G (2007) Role of the trigonal warping on the minimal conductivity of bilayer graphene. *Phys Rev Lett* 99:066802.
13. Moghaddam AG, Zareyan M (2009) Anisotropic minimal conductivity of graphene bilayers. *Phys Rev B* 79:073401.
14. Das Sarma S, Hwang EH, Rossi E (2010) Theory of carrier transport in bilayer graphene. *Phys Rev B* 81:161407.
15. Trushin M, Kailasvuori J, Schliemann J, MacDonald AH (2010) Finite conductivity minimum in bilayer graphene without charge inhomogeneities. *Phys Rev B* 82:155308.
16. Dávid G, Rakyta P, Oroszlány L, Cserti J (2012) Effect of the band structure topology on the minimal conductivity for bilayer graphene with symmetry breaking. *Phys Rev B* 85:041402.
17. McCann E, Fal'ko VI (2006) Landau-level degeneracy and quantum Hall effect in a graphite bilayer. *Phys Rev Lett* 96:086805.
18. Velasco J, Jr. (2012) Transport spectroscopy of symmetry-broken insulating states in bilayer graphene. *Nat Nanotechnol* 7:156–160.
19. Vafek O, Yang K (2010) Many-body instability of Coulomb interacting bilayer graphene: Renormalization group approach. *Phys Rev B* 81:041401(R).
20. Lemonik Y, Aleiner IL, Toke C, Fal'ko VI (2010) Spontaneous symmetry breaking and Lifshitz transition in bilayer graphene. *Phys Rev B* 82:201408(R).
21. Mayorov AS, et al. (2011) Interaction-driven spectrum reconstruction in bilayer graphene. *Science* 333:860–863.
22. Min H, Borghi G, Polini M, MacDonald AH (2008) Pseudospin magnetism in graphene. *Phys Rev B* 77:041407(R).
23. Zhang F, Min H, Polini M, MacDonald AH (2010) Spontaneous inversion symmetry breaking in graphene bilayers. *Phys Rev B* 81:041402(R).
24. Nandkishore R, Levitov L (2010) Dynamical screening and excitonic instability in bilayer graphene. *Phys Rev Lett* 104:156803.
25. Zhang F, Jung J, Fiete GA, Niu Q, MacDonald AH (2011) Spontaneous quantum Hall states in chirally stacked few-layer graphene systems. *Phys Rev Lett* 106:156801.
26. Nandkishore R, Levitov L (2010) Quantum anomalous Hall state in bilayer graphene. *Phys Rev B* 82:115124.
27. Jung J, Zhang F, MacDonald AH (2011) Lattice theory of pseudospin ferromagnetism in bilayer graphene: Competing interaction-induced quantum Hall states. *Phys Rev B* 83:115408.
28. Zhang F, MacDonald AH (2011) Distinguishing spontaneous quantum Hall states in bilayer graphene. *Phys Rev Lett* 108:186804.
29. Freitag F, Trbovic J, Weiss M, Schönenberger C (2012) Spontaneously gapped ground state in suspended bilayer graphene. *Phys Rev Lett* 108:076602.

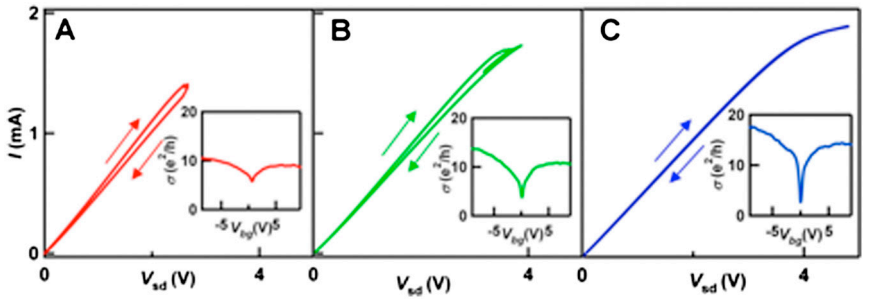

Fig. S1. Successive current-annealing cycles (from left to right) displayed in terms of I as a function of source-drain bias V_{sd}. (*Insets*) $\sigma(V_{bg})$ after each current-annealing cycle.

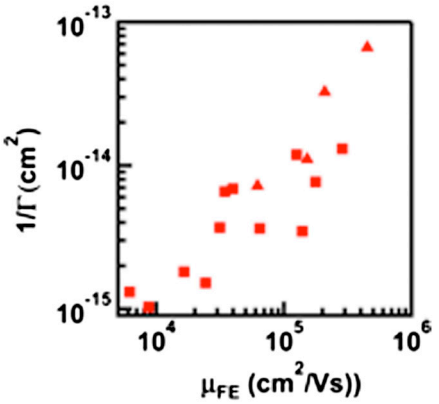

Fig. S2. Inverse FWHM of $\rho_c(n)$ urves as a function of μ_{FE}.

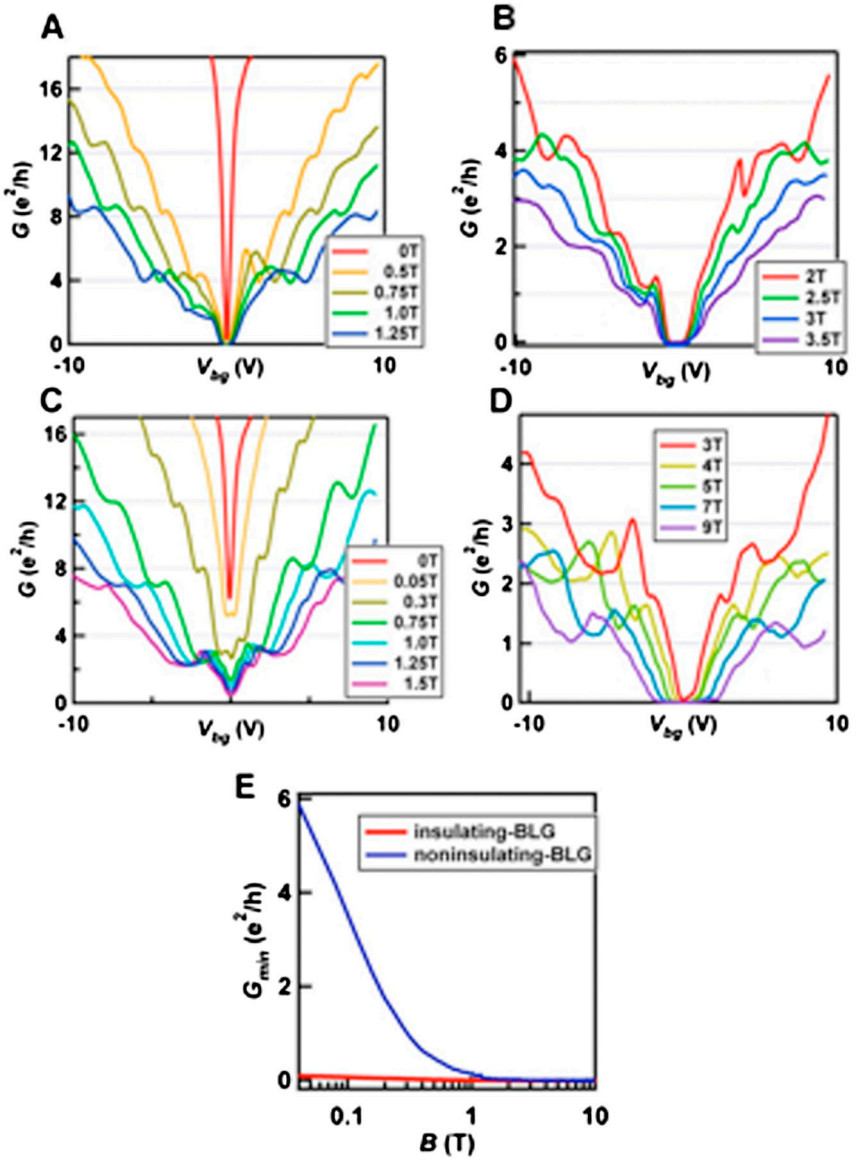

Fig. S3. (*A*–*D*) Line traces $G(V_{bg})$ taken at different magnetic fields in insets of Fig. 1*D* and *E*. (*E*) G_{min} as a function of *B* (in log scale) at CNP for suspended BLG devices shown in Fig. 1 *D* and *E*.

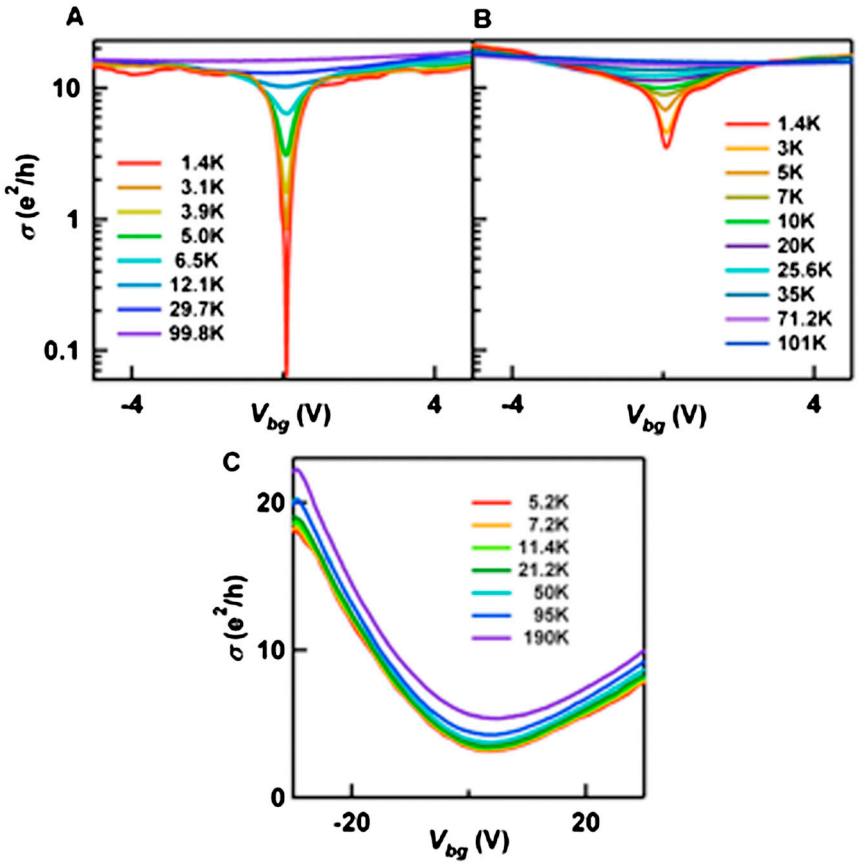

Fig. S4. (*A–C*) $\sigma(V_{bg})$ at different temperatures for suspended insulating, suspended non-insulating, and substrate-supported BLG devices, respectively.

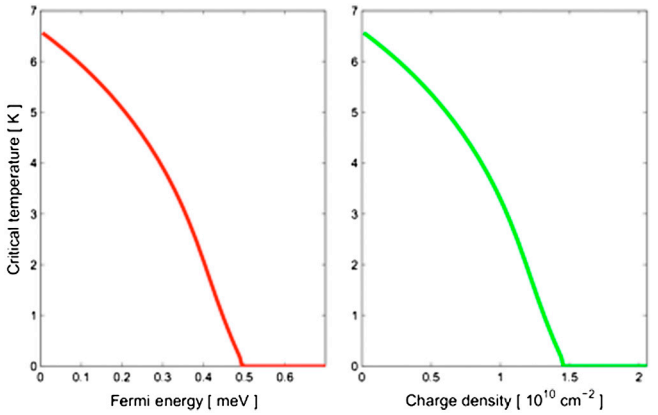

Fig. S5. Critical temperature T_c as a function of Fermi energy ε_F or charge carrier density n.

Table S1. Summary of minimum conductance (per square) σ_{min} in units of e^2/h at zerocarrierdensity of various non-interacting or symmetry-breaking bilayergraphene

States	Non-interacting without TR	Non-interacting with TR	Nematic order without TR	Nematic order with TR	QAH	QSH	LAF	QVH
gaps	gapless	gapless	gapless	gapless	gapped	gapped	gapped	gapped
σ_{min}	$\frac{8}{\pi}$	$\frac{24}{\pi}$	$\frac{8}{\pi}$	$\approx\frac{8}{\pi}$, anisotropic	4	4	$\ll 1$	$\ll 1$